Journal of Solid State Chemistry **148,** 286–294 (1999)
Article ID jssc.1999.8449, available online at http://www.idealibrary.com on IDEAL®

# Hydrothermal Synthesis, Structural, and Magnetic Studies of a New Fluoropyrophosphate: $BaFe^{II}_2P_2O_7F_2$

J.-M. Le Meins,* J.-M. Grenèche,† and G. Courbion‡

*Laboratoire de Matériaux Minéraux, UPRES-A 7016, Ecole Nationale Supérieure de Chimie de Mulhouse, 3, rue Alfred Werner, 68093 Mulhouse Cedex, France; †Laboratoire de Physique de l'Etat Condensé, UPRES-A 6087, Université du Maine, Faculté des Sciences, Av. O. Messiaen, 72085 Le Mans Cedex 09, France; and ‡Laboratoire des Fluorures, UPRES-A 6010, Université du Maine, Faculté des Sciences, Av. O. Messiaen, 72085 Le Mans Cedex 09, France

Received February 19, 1999; in revised form July 12, 1999; accepted July 22, 1999

**$BaFe_2(P_2O_7)F_2$ has been synthesized hydrothermally (24 h, 700°C). Its structure, determined using room-temperature single-crystal X-ray diffraction data, is othorhombic (space group *Pmmn*, No. 59) with cell parameters $a = 6.878(1)$ Å, $b = 11.847(2)$ Å, $c = 4.588(1)$ Å, $V = 373.9(1)$ Å$^3$, and $Z = 2$. The reliability factors converge to $R_1 = 2.0\%$ and $\omega R_2 = 5.8\%$ for 1267 unique reflections ($I > 2\sigma(I)$). The structure, which is compared to that of the minerals Lawsonite and Henomartinite, consists of octahedra infinite chains $[FeO_3F]^{5n-}_n$ and $P_2O_7$ pyrophosphate linked to generate a three-dimensional framework. Mössbauer data are consistent with the presence of one $Fe^{2+}$ site in the high spin state. Magnetic couplings are discussed in terms of superexchange and super-superexchange interactions.** 

*Key Words:* **hydrothermal synthesis; fluoropyrophosphates; superexchange; X-ray diffraction; Mössbauer spectrometry.**

## INTRODUCTION

Hydrothermal media seem to play an important role in the synthesis of fluorophosphate compounds with generic formula $AM_x(PO_4)_yF_z$. In order to point out this feature and synthesize new unknown oxyfluorinated frameworks or open frameworks, we have studied several systems (1). Most of them involved trivalent magnetic species (Fe) and alkaline-earth ones (Sr, Ba), in different hydrothermal media ($HF–H_2O–H_3PO_4$). During the study of the $xBaF_2/y\alpha$-$Fe_2O_3$ system, a new fluoropyrophosphate $BaFe_2(P_2O_7)F_2$ was obtained as by-product in the synthesis of $BaFePO_4F_2$ (2). In the present work, we report the characterization of $BaFe_2(P_2O_7)F_2$ and its magnetic properties are discussed.

## EXPERIMENTAL

### *Sample Preparation*

$BaFe_2(P_2O_7)F_2$ was synthesized hydrothermally from $BaF_2$ and $Fe_2O_3$ (molar ratio: 1/0.5) in an aqueous solution of phosphoric and fluorhydric acids (Labosi Analypur) with equal concentration of 4.7 M. The resulting mixture was introduced in a platinum tube with a filling level of approximately 45% according to the Kennedy table (3). This tube was sealed under argon and then placed in an autoclave submitted at room temperature to an external pressure of nitrogen (~80 MPa). The whole is heated up to 700°C during 24 h; the maximum pressure reached in such conditions was around 187 MPa. After cooling, the precipitate (totally crystallized) was filtered and washed thoroughly with distilled water and ethanol. The products consisted of at least two kinds of shiny crystals easily discernable with naked eyes upon color criteria. Under optical microscope, only two kinds of single-crystalline particles were observed. They revealed a similar shape (thin rectangular plates), dark green or translucent colorless. These last ones were identified as $BaFe_2(P_2O_7)F_2$ in weaker proportion (from 10 to 20% only) than the dark green plates of $BaFePO_4F_2$ (which is isotypic with $SrFePO_4F_2$ (2)).

### *Single-Crystal X-Ray Diffraction Measurement*

A single crystal of $BaFe_2(P_2O_7)F_2$ selected by optical examination and checked by Laue photography was mounted on a Siemens AED2 four-circle diffractometer, with monochromatized Mo$K\alpha$ radiation. The crystal system is orthorhombic with cell parameters $a = 6.878(1)$ Å, $b = 11.847(2)$ Å, $c = 4.588(1)$ Å determined from 32 reflections in the angular domain $28° < 2\theta < 32°$. The unit cell volume is 373.9(1) Å$^3$ with $Z = 2$. The systematic extinctions—$hk0$; $h + k = 2n$—are in agreement with the space group *Pmmn* (No. 59) and its non centrosymmetric subgroup $Pmn2_1$ (No. 31). Data collection was performed in the range $3° < 2\theta < 80°$ using the $\omega$-$2\theta$ scanning method ($N = 36$ steps of $\Delta\omega = 0.035°$) and no significant intensity decay (2.9%) was detected from standard reflections monitored every 60 mn. A total of 3622 reflections was collected but after merging only 1210 reflections with $I > 2\sigma(I)$ were used in the



0022-4596/99 $30.00

structure refinement (43 refined parameters). The introduction of absorption correction (face indexing absorption correction was applied) does not significantly improve the results when corrected data are used. The structure was solved using automatic Patterson interpretation (option PATT) of the program SHELXS-86 (4) (only the reflections in a limiting sphere of resolution of about 1 Å ($2\theta < 45^\circ$) were used for phase determination). Then the structure refinement was performed using the SHELXL-93 (5) crystallographic software. Crystal data and conditions of intensity measurement are listed in Table 1.

### *Characterization*

The infrared spectrum was collected with an ATI Mattson Genesis spectrometer. Fluorine analyses were realized by the pyrohydrolysis method (6).

The susceptibility measurements were carried out using a conventional Faraday balance calibrated with a cobalt mercurithiocyanate sample. The compound was zero field cooled from 300 to 4.2 K.

$^{57}$Fe transmission Mössbauer spectra were recorded with a constant acceleration spectrometer using a $^{57}$Co source diffused into a Rh matrix. The sample was located in a bath cryostat and the temperature accuracy was estimated to be 0.5 K. Velocity calibrations were performed using 99.99% pure 10 μm metallic iron foil. Isomer shift values are reported with respect to that of metallic iron foil at 300 K. The refinement used the least-squares MOSFIT program (7).

**TABLE 1**
**Crystallographic Data and Conditions of Intensities Collection for $BaFe_2(P_2O_7)F_2$**

| | |
|---|---|
| Crystal volume | $2.22 \times 10^{-3}$ mm$^3$ |
| Radiation | Mo$K\alpha$, $\lambda = 0.7109$ Å |
| Absorption coefficient $\mu$ | 97.6 cm$^{-1}$ |
| Crystal system | Orthorhombic |
| Space group | *Pmmn* (No. 59) |
| Volume/$Z$ | 373.9(1) Å$^3$/2 |
| Cell dimensions | $a = 6.878(1)$ Å |
| | $b = 11.847(2)$ Å |
| | $c = 4.588(1)$ Å |
| Density (calculated) | 4.09 g cm$^{-3}$ |
| Cell parameters refined from | 32 reflections measured in a double step scan at $\pm 2\theta \approx 30^\circ$ |
| Data collection range | $3.00^\circ \leq 2\theta \leq 80.00^\circ$ |
| Range of measurement $h$, $k$, $l$ | $-12 \leq h \leq 12$ |
| | $-21 \leq k \leq 21$ |
| | $-8 \leq l \leq 8$ |
| Counter aperture | 4 × 4 mm |
| Number of collected intensities | 3622 |
| Max. intensity standard variation | 2.9% |
| Number of independent reflections | 1267 ($R_{int} = 2.8\%$) |
| Independent reflections ($I > 2\sigma(I)$) | 1210 |
| Number of refined parameters | 43 |
| Secondary extinction correction[a] | 0.056(2) |
| Weighting scheme[a] | $1/[\sigma^2(F_o^2) + (0.0286 \times P)^2 + 0.418P]$ |
| Final Fourier residuals | $-1.85$ to 1.57 e$^-$/Å$^3$ at 0.58 Å from $Ba^{2+}$ |
| $R_1/\omega R_2$[a] | 0.020/0.058 |

[a] As defined in SHELXL-93 (5).

## RESULTS AND DISCUSSION

### *Refinement*

The structure was determined and refined in the centrosymmetric space group *Pmmn* (No. 59). The Ba atom, the Fe ones, and one oxygen atom were first located by the automatic Patterson interpretation. The P atom and all the anions of the structure considered as oxygen are localized after several successive examinations of difference Fourier maps and upon interatomic distance criteria. The agreement factors drop very quickly to $R_1(F_o) = 4.9\%$ and $\omega R_2(F_o^2) = 13.9\%$. The refinement of anisotropic atomic displacement parameters (ADPs) yields $R_1 = 2.4\%$ and $\omega R_2 = 7.1\%$.

At this step of refinement, the neutral formula $BaFe_2^{III}P_2O_9$ is obtained. *A priori*, the agreement factors seem good. Nevertheless, a careful examination of the ADPs associated to one oxygen atom (O) reveals rather weak values, but not weak enough to generate a nonpositive $\beta$ matrix. On the basis of both these agreement factors and the resulting crystallographic model (with no abnormal interatomic distances), the bond valence sum (8) was established for the hypothetical formula $BaFeP_2O_9$. The results are given in Table 2. Two main observations can be made: first, the calculated valence for the $O^{2-}$ anion is only 1.01 v.u., characteristic of a $F^-$ anion (a hydroxyl group $OH^-$ should have given a value of 1.2 v.u.), and second, the $Fe^{3+}$ cation shows a valence of only 2.18 v.u. This implies that the iron oxidation state in the compound is II (this will be confirmed by Mössbauer spectrometry) and that two oxygen atoms have to be replaced by fluorine ones.

The substitution of O by F and the introduction of scattering coefficients corresponding to the $Fe^{2+}$ cation allow a relative decrease of the $R_1$ factor for more than 14%: $R_1 = 2.0\%$ and $\omega R_2 = 5.8\%$ for 1267 unique reflections and 43 refined parameters.

The final atomic coordinates, selected bond distances for the formula $BaFe_2(P_2O_7)F_2$, are listed in Tables 3 and 4 respectively.

### *Chemical Analyses*

The results of both an X-ray experiment and a valence bond calculation show clearly that a partial reduction of iron III took place in the platinum tube during the hydrothermal synthesis. This reduction is only partial because it must be remembered that the major phase observed is $BaFe^{III}PO_4F_2$. Such a reduction phenomenon is quite often observed (9–11) even in a sealed tube and is explained by

**TABLE 2**
**Bond Valence Analysis for the Formula $BaFe_2P_2O_9$**

| Atom | Ba | $Fe^{3+}$ | P | $\sum s$ | Charge |
|---|---|---|---|---|---|
| O | $0.309^{\times 2\downarrow}_{\times 1\rightarrow}$ $0.202^{\times 2\downarrow}_{\times 1\rightarrow}$ | $0.251^{\times 2\downarrow}_{\times 2\rightarrow}$ | — | **1.013** | **2** |
| O(1) | — | $0.356^{\times 2\downarrow}_{\times 2\rightarrow}$ | 1.255 | **1.967** | **2** |
| O(2) | $0.320^{\times 4\downarrow}_{\times 1\rightarrow}$ | $0.481^{\times 2\downarrow}_{\times 1\rightarrow}$ | $1.272^{\times 2\downarrow}_{\times 1\rightarrow}$ | **2.073** | **2** |
| O(3) | — | — | $0.981^{\times 2\downarrow}_{\times 1\rightarrow}$ | **1.962** | **2** |
| $\sum s$ | **2.302** | **2.176** | **4.780** | — | — |
| Charge | **2** | **3** | **5** | — | — |

*Note*. The arrows indicate the way in which the multiplicative coefficient must be taken into account for the final summation. The values are issued from the equation $s = \exp[(R_0 - d)/0.37]$ with $R_0 = 2.29$, 1.759, and 1.604 for $Ba^{2+}$–O, $Fe^{3+}$–O, and $P^{5+}$–O, respectively.

traces of water outside the platinum tube, between the tube and the steel lining of the autoclave. Metallic iron from steel is then oxidized with hydrogen production which allows the reduction of iron III. This water can be brought in by moist nitrogen which applies external counterpressure.

In order to check the absence of any substitution of $F^-$ anions by $OH^-$ groups (although it has been shown here that X-ray experiment results were efficient to make a clear distinction), two kinds of experiments were carried out each time on single crystals: fluorine analyses and IR recording. The results of fluorine analysis are in good agreement with the formula issued from the X-ray experiment. The experimental weight percentage of fluorine is 7.8(1)% (8.24% expected for 2 $F^-$ per formula). IR spectrum was recorded from 500 to 4000 $cm^{-1}$ and confirms unambiguously the absence of $OH^-$ groups (no large band around 3000 $cm^{-1}$). Such a spectrum is characteristic of the presence of $[P_2O_7]$ bitetrahedron units: the bands from 1100 to 1200 $cm^{-1}$ and from 400 to 600 $cm^{-1}$ concern $PO_3$ vibrators, whereas the band at 950 $cm^{-1}$ can be attributed to $\upsilon_{as}$P–O–P and finally the sharp band around 750 $cm^{-1}$ to $\upsilon_s$P–O–P (12).

**TABLE 3**
**Atomic Coordinates and Equivalent Isotropic Displacement Parameters $B_{eq}$ for $BaFe_2(P_2O_7)F_2$,**
$$B_{eq} = \frac{8\pi^2}{3} = \sum_i \sum_j U_{ij} a_i^* a_j^* a_i a_i$$

| Atom | Site | Site factor occupation | $x$ | $y$ | $z$ | $B_{eq}$ (Å$^2$) |
|---|---|---|---|---|---|---|
| Ba | 2*b* | 0.25 | $\frac{1}{4}$ | $\frac{3}{4}$ | 0.38923(4) | 0.729(5) |
| Fe | 4*c* | 0.5 | 0 | 0 | 0 | 0.623(5) |
| P | 4*e* | 0.5 | $\frac{1}{4}$ | 0.12589(4) | 0.5118(1) | 0.447(7) |
| O(1) | 4*e* | 0.5 | $\frac{1}{4}$ | 0.4519(1) | 0.2491(3) | 0.75(2) |
| O(2) | 8*g* | 1.0 | 0.06542 | 0.3835(1) | − 0.3093(2) | 0.80(1) |
| O(3) | 2*a* | 0.25 | $\frac{1}{4}$ | $\frac{1}{4}$ | 0.3686(5) | 0.78(3) |
| F | 4*e* | 0.5 | $\frac{1}{4}$ | 0.6144(1) | − 0.1316(3) | 1.09(2) |

**TABLE 4**
**Main Interatomic Distances in (Å) and Angles (°) in $BaFe_2(P_2O_7)F_2$**

Fe octahedron, site symmetry: $\bar{1}$

| Fe | O(2) | O(2) | O(1) | O(1) | F | F |
|---|---|---|---|---|---|---|
| O(2) | **2.030(1)** | 4.060(2) | 2.930(2) | 2.972(2) | 3.124(3) | 2.966(2) |
| O(2) | 180 | **2.030(1)** | 2.972(2) | 2.930(2) | 2.966(2) | 3.124(3) |
| O(1) | 89.18(5) | 90.82(5) | **2.142(1)** | 4.283(2) | 3.568(2) | 2.599(2) |
| O(1) | 90.82(5) | 89.18(5) | 180 | **2.142(1)** | 2.599(2) | 3.568(2) |
| F | 92.98(5) | 87.02(5) | 107.89(5) | 72.11(5) | **2.271(1)** | 4.542(2) |
| F | 87.02(5) | 92.98(5) | 72.11(5) | 107.89(5) | 180 | **2.271(1)** |

⟨Fe–O, F⟩ 2.15 Å, $d_{Shannon}$ 2.11 Å (14)

P tetrahedron, site symmetry: *m*

| P(1) | O(2) | O(2) | O(1) | O(3) |
|---|---|---|---|---|
| O(2) | **1.516(1)** | 2.538(3) | 2.524(2) | 2.509(2) |
| O(2) | 113.7(1) | **1.516(1)** | 2.524(2) | 2.509(2) |
| O(1) | 112.68(5) | 112.68(5) | **1.518(2)** | 2.454(2) |
| O(3) | 106.74(6) | 106.74(6) | 103.3(1) | **1.611(1)** |

⟨P–O⟩ 1.54 Å, $d_{Shannon}$ 1.52 Å

Ba polyhedron

| | |
|---|---|
| Ba–O(2) | 2.710(1) |
| Ba–O(2) | 2.710(1) |
| Ba–O(2) | 2.710(1) |
| Ba–O(2) | 2.710(1) |
| Ba–F | 2.723(2) |
| Ba–F | 2.723(2) |
| Ba–F | 2.879(2) |
| Ba–F | 2.879(2) |

⟨Ba–O, F⟩ 2.75 Å, $d_{Shannon}$ 2.74 Å

*Description and Structural Relationships*

Figure 1 (13) depicts the polyhedral representation of $BaFe_2(P_2O_7)F_2$. The three-dimensional framework consists of two polyhedral types: $[FeO_4F_2]$ octahedra and $[P_2O_7]$ pyrophosphates. Bond distances and angles for the polyhedra are listed in Table 4. By sharing two opposite edges, Fe II octahedra form infinite chains $[FeO_3F]_n^{5n-}$ running parallel to the [100] axis. The main original feature of this new pyrofluorophosphate is the mixed (O, F) nature of the shared edge. The interchain linkage is made by diphosphate units. In Table 4, the distance P–O(3) of 1.611 Å is larger than the other P–O distances (14); it is characteristic of the O(3) vertex bridging the two tetrahedra. The main axis of the pyrophosphate P–O(3)–P is oriented along [010]. Such an orientation leads to connections between the iron chains via the $[P_2O_7]$ unit along [010], while ones standing in the (001) plane are connected by the tetrahedra (Fig. 2).

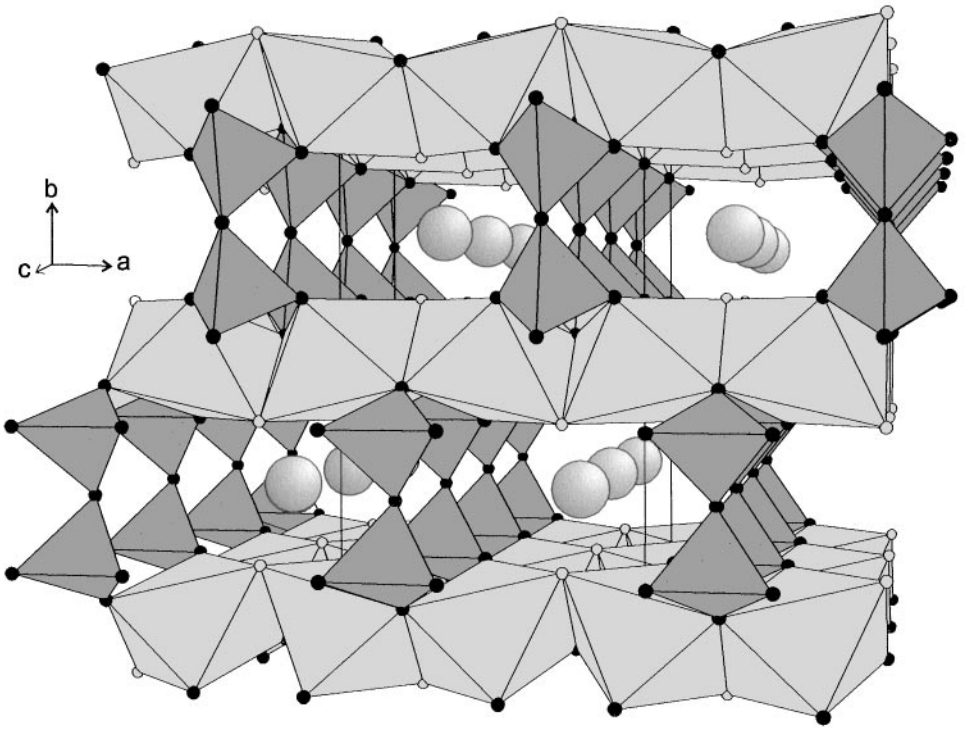


**FIG. 1.** [001] perspective view of $BaFe_2(P_2O_7)F_2$ (large gray spheres are $Ba^{2+}$ cations, small black or gray ones are $O^{2-}$ or $F^-$, respectively).

This topology generates small channels in both directions [100] and [001]. Along [001], the aperture presents dimensions around $6.88 \times 3.16$ Å whereas along [100] a smaller aperture is observed: $4.59 \times 3.16$ Å. In the resulting cavities (channels crossing over) are inserted the $Ba^{2+}$ cations, inside a pseudocubic polyhedron. It is worth noting a slight shift of the $Ba^{2+}$ position in relation to the center of the cavity. This can be explained by the spatial constraints dictated by two $F^-$ neighbor anions pointing toward the middle of the cavity. Such a shift involves that $Ba^{2+}$ being surrounded by two $F^-$ from the adjacent cavity and four $O^{2-}$ and two $F^-$ from its own cavity, with distances ranging from 2.710 to 2.879 Å.

As mentioned in the Introduction, this structure presents similar topological characteristics with the following two minerals: Lawsonite $Ca[Al_2(Si_2O_7)(OH)_2]$-$H_2O$ (15) and Henomartinite $Sr[Mn_2(Si_2O_7)(OH)_2]$-$H_2O$ (16). In these minerals, $[Si_2O_7]$ bitetrahedra connect the infinite chains $[AlO_3(OH)]_n$ or $[MnO_3(OH)]_n$. However, some differences can be noted. Table 5 allows a fast comparison of the main crystallographic characteristics between the two minerals and our synthetic fluorinated compound. Two main differences can be pointed out. First, the presence of a water molecule inside the cavities involves a large modification of the $A^{2+}$ coordination polyhedron: an octahedron for $Ca^{2+}$ and a bicapped octahedron for $Sr^{2+}$ instead of a pseudocubic polyhedron for $Ba^{2+}$. Second, some supplementary bitetrahedron units suppress the channels in the *b*-direction for the Lawsonite. This last observation can be correlated to the C Bravais lattice which implies a doubling of the *b*-parameter in comparison to the *c*-parameter of $BaFe_2(P_2O_7)F_2$. Consequently, along the *b*-axis two successive chains are different for the Lawsonite structure whereas they are the same for $BaFe_2(P_2O_7)F_2$ (along the *c*-axis). This allows supplementary connections with the $[Si_2O_7]$ bitetrahedra, according to the alternation of O/OH vertices along [010]. The existence of channels along [001] for $BaFe_2(P_2O_7)F_2$ results from forbidden connections of tetrahedra via a fluorine atom.

One notices that other fluorophosphates such as $K_2M_2(P_2O_7)F_2$ ($M = Fe^{2+}$, $Mn^{2+}$) have been investigated by Yakubovitch *et al.* (17, 18). Nevertheless their structure is very different from that of $BaFe_2(P_2O_7)F_2$. The zig-zag chains of octahedra (connected via $[P_2O_7]$ units) result from the sharing of mixed O–F edges in *cis* position; thus, there are no channels in these structures.

### *Susceptibility Measurements and Mössbauer Results*

The thermal variation of the inverse susceptibility is shown in Fig. 3. Above 10 K the curve shows a quasi-linear evolution and follows a Curie–Weiss law leading to a weak paramagnetic Curie temperature value: $\theta_p = -9(5)$ K. Below 10 K no ordering temperature can be evidenced.

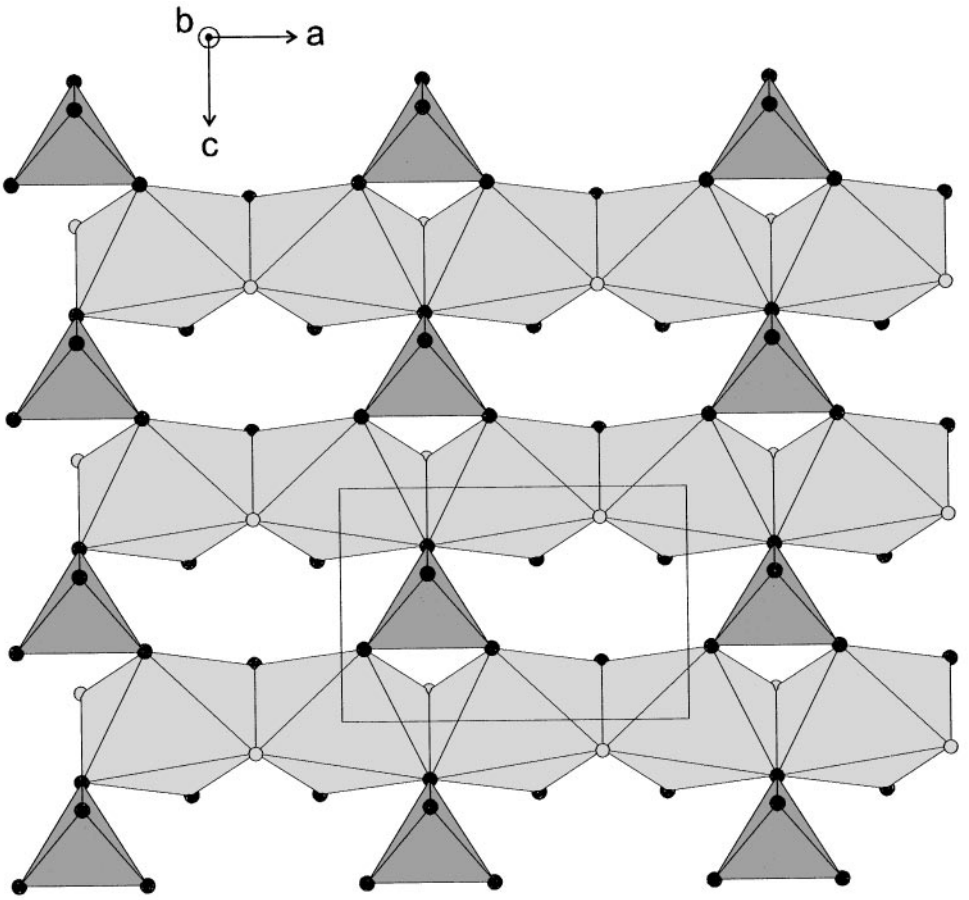


**FIG. 2.** (010) projection ($-0.12 < y < +0.25$) illustrating the chain connections via [$PO_4$] unit.

The experimental effective moment, 4.89 $\mu_B$ for one $Fe^{2+}$ ($3d^6$), is in fair agreement with the calculated one (only spin contribution).

**TABLE 5**
**Compounds Related to $BaFe_2(P_2O_7)F_2$**

| Formula | Lawsonite (15) $Ca[Al_2(Si_2O_7)(OH)_2]$–$H_2O$ | Henomartinite (16) $Sr[Mn_2(Si_2O_7)(OH)_2]$–$H_2O$ | $Ba[Fe_2(P_2O_7)F_2]$ |
|---|---|---|---|
| Crystal system | Orthorhombic | Orthorhombic | Orthorhombic |
| Space group | *Cmcm* (No. 63) | *Cmcm* (No. 63) | *Pmmn* (No. 59) |
| Cell parameters | $a = 5.85$ Å<br>$b = 8.79$ Å<br>$c = 13.14$ Å | $a = 6.25$ Å<br>$b = 9.03$ Å<br>$c = 13.40$ Å | $a = 6.88$ Å<br>$b = 11.85$ Å<br>$c = 4.59$ Å |
| Octahedra formula[a] | $AlO_2\mathbf{O_2(OH)_2}$ | $MnO_2\mathbf{O_2(OH)_2}$ | $FeO_2\mathbf{O_2F_2}$ |
| Inserted species and coordination | $Ca^{2+}$<br>[6]: $Ca(H_2O)O_5$ | $Sr^{2+}$<br>[8]: $Sr(H_2O)O_7$[b] | $Ba^{2+}$<br>[8]: $BaO_4F_4$ |

[a] Anions which allow the connections of the octahedra inside a chain are bold-faced.

[b] Water molecule is on 8*g* site, half occupied (instead of a 4*c* fully occupied position for the Lawsonite). The positions are 0.043, 0.607, $\frac{1}{4}$ (8*g* site) (16) and 0, 0.610, $\frac{1}{4}$ (4*c* site) (15).

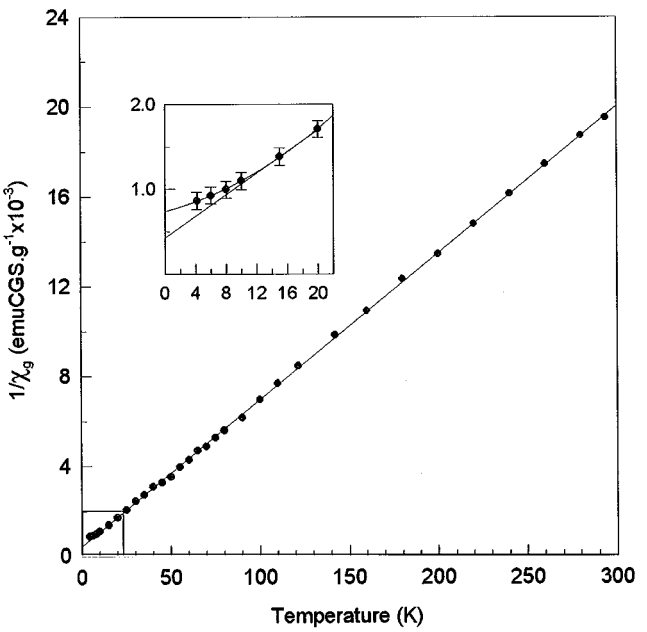


**FIG. 3.** Thermal variation of the inverse susceptibility for $BaFe_2(P_2O_7)F_2$.

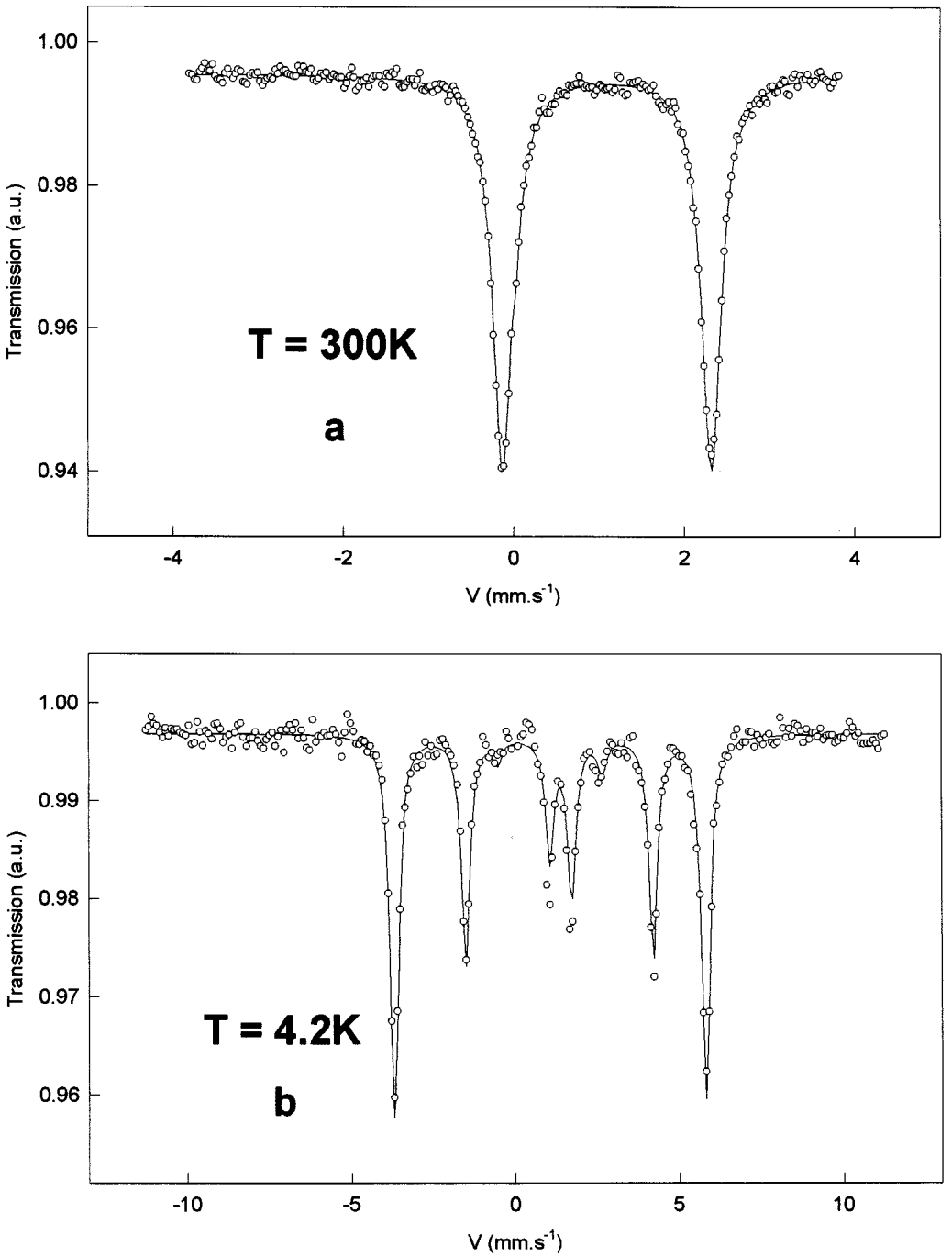


**FIG. 4.** Mössbauer spectra at (a) 300 K and (b) 4.2 K.

Mössbauer experiments allow us to show a magnetic order temperature close to 10 K. Selected Mössbauer spectra recorded either in the paramagnetic or in the magnetic range are illustrated in Fig. 4. At 300 and 77 K, they show a quadrupolar doublet with narrow lines. The refined values of hyperfine parameters, listed in Table 6, are characteristic of a $Fe^{2+}$ cation in an octahedral site with high spin state. Moreover, the decrease of the quadrupolar splitting with increasing temperature confirms the presence of $Fe^{2+}$ cations, consistently with the bond valence calculation discussed in the above section.

The spectrum recorded at 4.2 K shows a pure magnetic sextet. The hyperfine field 26.6(3) T is consistent with that expected in the case of divalent iron (25–30 T). The value of

**TABLE 6**
**Hyperfine Parameters in Paramagnetic and Magnetic Range for $BaFe_2P_2O_7F_2$**

| $T$ (K) | IS ($mm \cdot s^{-1}$) | $\Gamma$ ($mm \cdot s^{-1}$) | $\Delta$ or $2\varepsilon$ ($mm \cdot s^{-1}$) | $\eta$ | $\theta$ (°) | $\gamma$ (°) | $H_{hf}$ (T) |
|---|---|---|---|---|---|---|---|
| 300 | 1.22(1) | 0.28(1) | 2.42(1) | — | — | — | — |
| 77 | 1.33(1) | 0.27(1) | 2.53(1) | — | — | — | — |
| 10 | 1.37(1) | 0.40(1) | 2.64(1) | — | — | — | — |
| 4.2 | 1.37(1) | 0.31(1) | 2.56(1) | 0.6 | 80(5) | 58(5) | 26.6(3) |

*Note*. IS is the isomer shift given relative to that of metallic iron at 300 K, $\Gamma$ the line width at half height, $\Delta$ the quadrupolar splitting, $2\varepsilon$ the quadrupolar shift ($2\varepsilon = \Delta/2(3\cos^2\theta - 1)$), $\eta$ the asymmetry parameter defined as $|(V_{xx} - V_{yy})/V_{zz}|$ assuming, $|V_{xx}| \leq |V_{yy}| \leq |V_{zz}|$, $\theta$ and $\gamma$ the polar angles of the hyperfine field in the EFG coordinate system, and $H_{hf}$ the hyperfine field.

asymmetry parameter $\eta$ (see Table 6 for definition) clearly evidences for a nonaxial electric field gradient. The spectrum recorded at 10 K shows a slightly asymmetric doublet and broader lines than at higher temperature ($\Gamma = 0.40(1)\ mm \cdot s^{-1}$); this is consistent with the onset of a magnetic ordered behavior. As a matter of fact, a spectrum recorded at 9 K, showing unambiguously a magnetic hyperfine structure, indicates that the Néel temperature (not observed in the susceptibility measurements) is close to 10 K.

The weak value of $\theta_p$ is indicative of very weak dominant antiferromagnetic couplings and is also consistent with the presence of both antiferromagnetic and ferromagnetic interactions. The interactions originate from the classical superexchange (SE) coupling (edge sharing) inside the chains of $Fe^{2+}$. However, super-superexchange (SSE) couplings via $[PO_4]$ tetrahedra are expected between two adjacent chains standing in the (010) plane and are also possible inside a chain (Fig. 5). Each $Fe^{2+}$ octahedron is surrounded by two octahedra in the chains and is also linked to six other octahedra belonging to adjacent chains. A total of fourteen interactions may be counted; four kinds are listed in Table 7. Taking simple and double pathways for both superexchange and super-superexchange interactions into account, there are ten SSE couplings and four SE interactions.

The expected SE couplings (J) inside a chain ($Fe^{2+}$ cations at $d = 3.4$ Å) will be the stronger ones, but less numerous. According to the connection mode between octahedra, two kinds of orbital overlap can be considered (19, 20): $e_g$-$p$-$t_{2g}$ and $e_g$-$p_\sigma$-$p_{\sigma'}$-$e_g$. This last one favors a ferromagnetic coupling, which competes with the antiferromagnetic contributions involved by the $e_g$-$p$-$t_{2g}$ overlap. Both interactions might contribute to a weak antiferromagnetic behavior in the chains. The 2D magnetic coupling (in the (010) plane) is assumed by the antiferromagnetic SSE interactions between chains. Among the ten SSE interactions (corner sharing), the stronger ones correspond to those having superexchange angles not too far from 180°: $J'_{L1} \gg J'_{L2} \approx J'_C$. Owing to the large distances between chains connected by the $[P_2O_7]$ pyrophosphate along the $b$-direction and the weak angle (O–O–O = 78°) the magnetic couplings involving super-super-superexchange ($Fe^{2+}$–O–O–O–$Fe^{2+}$) in this direction can be neglected. With only two main magnetic coupling constants, $J$ and $J'_{L1}$, a simple antiferromagnetic model (Fig. 6) can be derived for $BaFe_2(P_2O_7)F_2$, consistently with the susceptibility measurements.

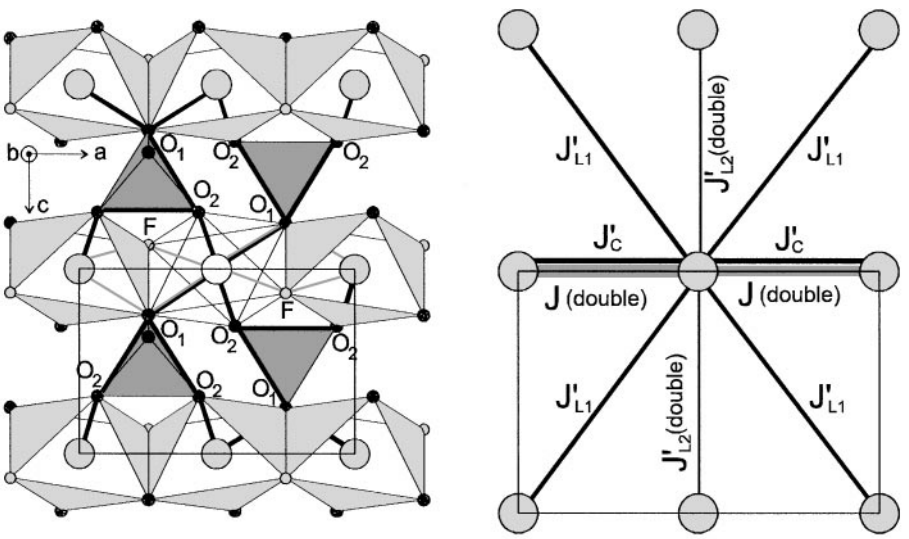


**FIG. 5.** Magnetic interaction pathways (left) and coupling constants (right) for $BaFe_2(P_2O_7)F_2$.

**TABLE 7**
**Super Exchange (SE) and Super-superexchange (SSE) Angles and Distances between Two Magnetic Centers in $BaFe_2(P_2O_7)F_2$**

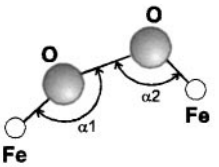


| Nature of interaction | Coupling constant and multiplicity | Number | Angles (°) | Distances between magnetic centers (Å) |
|---|---|---|---|---|
| SE | $J$ (double) | 2 | Fe–F–Fe = 98.4<br>Fe–O–Fe = 106.8 | 3.4 |
| SSE long distance | $J'_{L1}$ (single) | 4 | $117 < \alpha1, \alpha2 < 157$ | 5.7 |
| SSE long distance | $J'_{L2}$ (double) | 2 | $96 < \alpha1, \alpha2 < 117$ | 4.6 |
| SSE short distance | $J'_C$ (simple) | 2 | $\alpha1 = \alpha2 = 103$ | 3.4 |

*Note*. *L*, long distance; *C*, short distance. Number indices, multiplicity, $J'$, SSE coupling constant.

## CONCLUSION

Among the synthetic fluoropyrophosphates, $BaFe_2(P_2O_7)F_2$ seems to be the first example of compound inserting alkaline-earth species. Its structure is different from those of the $K_2M_2(P_2O_7)F_2$ phases ($M = Fe^{2+}$, $Mn^{2+}$) studied by Yakubovitch *et al*., but is related to those of the minerals Lawsonite and Henomartinite. The analysis of the topology reveals several kinds of weak contributions, either antiferromagnetic or ferromagnetic, leading to a dominant antiferromagnetic behavior. Such a phase is of interest for evidencing the role of the SSE couplings in the magnetic behavior. In this aim, magnetic structure determination is planed.

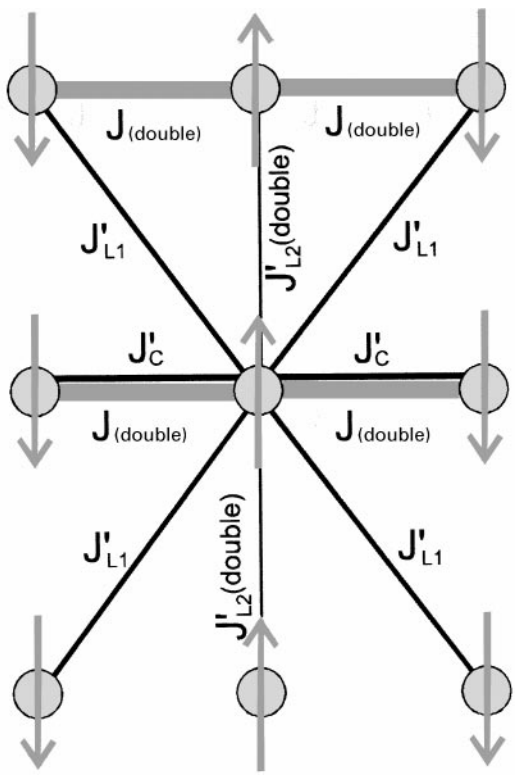


**FIG. 6.** Hypothetical magnetic structure for $BaFe_2P_2O_7F_2$ with an antiferromagnetic SE coupling constant (J) and with SSE interactions governed by $J'_{L1}$ (antiferromagnetic).

## ACKNOWLEDGMENT

The authors are indebted to Pr. M. Leblanc for his help in data collection.

## REFERENCES

1. J.-M. Le Meins, *Thesis*, Université du Maine, 1998.
2. J.-M. Le Meins, A. Hémon-Ribaud, Y. Laligant, and G. Courbion, *Eur. J. Solid State Inorg. Chem.* **34,** 391 (1997).
3. G. C. Kennedy, *Econ. Geol.* **45,** 629 (1950).
4. G. M. Sheldrick, SHELXS-86 *in* "Crystallographic computing 3" (G. M. Sheldrick, C. Krüger, and R. Coddard, Eds.), p. 175. Oxford University Press, Oxford, 1985.
5. G. M. Sheldrick, "SHELXL-93, A Program for Crystal Structure Determination." University of Göttingen, 1993.
6. J. C. Warf, W. D. Cline, and R. D. Tevebaugh, *Anal. Chem.* **26,** 342 (1954).
7. J. Teillet and F. Varret, MOSFIT, unpublished program.
8. N. Brese and O. Keeffe, *Acta Crystallogr. B* **47,** 192 (1991).
9. V. A. Kuznetsov, *J. Cryst. Growth* **3–4,** 405 (1968).
10. S. Mirano and S. Somiya, *J. Cryst. Growth* **35,** 273 (1973).
11. M. Leblanc, *Thesis*, Université du Maine, 1984.
12. V. Vincent, C. Breandon, G. Nihoul, and J. R. Gavarri, *Eur. J. Solid State Inorg. Chem.* **34,** 571 (1997).
13. K. Brandenburg and M. Berndt, "DIAMOND 2.0, Visual Crystal Structure Information System." Crystal Impact, Bonn, Germany.
14. R. D. Shannon, *Acta Crystallogr. A* **32,** 751–767 (1976).

15. W. H. Baur, *Am. Mineral.* **63,** 311 (1978).
16. T. Armbruster, R. Oberhänsti, and V. Bermanec, *Eur. J. Mineral.* **4,** 17 (1992).
17. O. V. Yakubovich, O. A. Evdokimova, and O. K. Mel'Nikov, *Dok. Akad. Nauk.* **1984,** 625 (1984).
18. O. V. Yakubovitch and O. K. Mel'Nikov, *Kristallografiya* **36,** 334 (1991).
19. J. Kanamori, *J. Phys. Chem. Solids* **10,** 87 (1959).
20. J. B. Goodenough *in* "Magnetism and the Chemical Bond." Interscience–Wiley, New York, 1963.